Adsorption and Diffusion of Fe on a Titania Ultrathin Film†

Giovanni Barcaro and Alessandro Fortunelli*

Molecular Modeling Laboratory, IPCF/CNR, via G. Moruzzi 1, Pisa I56124, Italy

Received: May 28, 2009; Revised Manuscript Received: September 10, 2009

The phenomenology of the adsorption of Fe adatoms and addimers and the diffusion of Fe adatoms on an ultrathin titanium oxide monolayer grown on the Pt(111) surface is investigated via density functional simulations. It is found that (i) Fe atoms adsorb on 3-fold hollow sites or defective holes of the oxide slab with interaction energies ranging from 2.3 to 4.7 eV; (ii) Fe dimers adsorb with a proportional energetics and a clear preference for horizontal rather than vertical configurations; (iii) Fe atoms diffuse over the oxide surface with energy barriers ranging from ∼0.7−1.1 eV on the compact regions to ∼1.6−2.0 eV on the defective regions of the film. All this points to a great importance of kinetic effects in the growth of Fe clusters on this surface, much greater than in the previously investigated cases of noble or quasi-noble metals such as Au and Pd.

I. Introduction

Dynamic processes during the growth process can have a fundamental importance in orienting the structure and morphology of metal particles. Their influence has been clearly proven for gas-phase aggregates,[1] and also for particles in a complex environment, such as metal clusters coated in the homogeneous phase[2,3] or deposited on an oxide substrate.[4] Especially for deposited particles, however, despite their scientific and technological interest in catalysis, chemical sensors, and other fields,[5] it is only in recent years that simulation studies have appeared on dynamic phenomena such as diffusion or melting; see, for example, refs 6 and 7. As for diffusion and growth, the attention has been initially focused on the mobility of adatoms and small clusters on model oxide surfaces, leading to predictions in very good agreement with available experimental data.[8−10] The next challenge is then associated with the study of more complex substrates, among which ultrathin oxide films (i.e., oxide films of thickness up to few nanometers) grown on single crystal metal surfaces present many reasons of interest. First, ultrathin films are conductive to some extent and can thus be characterized with atomistic resolution by probes involving charged particles, such as STM.[11] Second, these systems are new materials exhibiting novel phases that have no counterpart in the bulk.[12] In particular for polar films[13] (i.e., presenting alternating layers of metal and oxygen ions and thus a finite dipole moment perpendicular to the surface), the interplay between polarity and lattice mismatch at the metal−support/oxide-film interface makes that they are often modulated into regular nanostructured patterns.[14] Such patterns may also open up into point defects which act as trapping and nucleation centers for the growth of adsorbed species,[15,16] thus constituting nearly ideal nanotemplates; see, for example, ref 17. Third, the vicinity of the metal support can induce novel phenomena, such as the possibility of a charge transfer between the underlying metal surface and deposited Au aggregates.[18−21] It is thus of great interest to investigate the adsorption properties and the energy landscape of metal atoms diffusing on ultrathin polar oxide surfaces and to compare them with more traditional systems to see which phenomena are generated by the nanoscale confinement of the oxide layer, the presence of the underlying metal support, and the electrostatic effects associated with the polar character of the film. In this context, a titanium oxide (titania) ultrathin film grown on the Pt(111) surface (hereafter referred to as z'-TiO_x, as in the original reference[22]) is a particularly suitable substrate for such a study. In fact, the z'-TiO_x/Pt(111) system is a polar film, whose structure has been solved[23] and shown to be constituted of an interfacial layer of Ti ions and a topmost overlayer of O ions, the dimensions of its unit cell are not excessive by modern computational standards allowing one to develop systematic investigations, and its surface presents a varied topography, alternating compact pseudoepitaxial regions (stripes) and sparser, defective channels (troughs) in which Ti vacancies are found in the form of holes that cross the oxide film down to the bare Pt(111) support.

The first exploratory simulations of the diffusion of Au and Pd adatoms on the z' and other TiO_x/Pt(111) surfaces have been reported.[15,24,25] Here we focus on a rather different element (Fe) and analyze in detail the features of the adsorption and diffusion of single atoms and dimers on the z'-TiO_x/Pt(111) phase. Fe is chosen for its importance in catalysis and as a representative of a true transition metal to be contrasted with the thoroughly investigated noble metal Au or quasi-noble metal Pd. We find that Fe atoms diffusing on the z'-TiO_x/Pt(111) phase experience a rather irregular energy landscape with an overall strong adhesion to the surface, particularly intense in the vicinity of the defective regions, which suggests that the growth of Fe particles on this surface is subjected to strong kinetic control under the usual deposition conditions, at variance with the Au and Pd cases.

II. Computational Details

Density functional (DF) local optimizations are performed using the ESPRESSO package,[26] employing ultrasoft pseudopotentials[27] and the Perdew−Burke−Ernzerhof (PBE) exchange-correlation functional.[28] Note that we deem a gradient-corrected exchange-correlation functional to be appropriate for these oxide ultrathin phases, for which the presence of the underlying metal support and the conductive character resulting from the metal-

† Part of the "Vincenzo Aquilanti Festschrift".

* To whom correspondence should be addressed. E-mail: fortunelli@ipcf.cnr.it.

10.1021/jp904998c © 2009 American Chemical Society
Published on Web 10/05/2009

lization of the oxide layer as the depolarization mechanism may discorage the use of DFT + U or hybrid[29] methods that have recently been proposed for (defected or doped and in this sense reduced) stoichiometric titania phases[30,31] (further studies are in progress to clarify this point). We use numerical parameters similar to those employed in ref 15, such as 30 Ryd for the energy cutoff for the selection of the plane wave basis set for describing the wave function and 150 Ry for describing the electronic density (1 Ryd = 13.606 eV), respectively, and about 8−10 Å of empty space between replicated cells. The sampling of the first Brillouin zone is performed at the Γ point only, having verified in several cases that this approximation does not influence the accuracy of the obtained results with respect to the employment of the denser (2,4,1) k_{mesh} grid previously used. All the calculations are performed spin-unrestricted. The support is described using 2 layers of Pt, but this choice has been validated by comparison with calculations using 4 layers of Pt, which produced qualitatively similar results (as it is reasonable, due to the minor importance of image-charge effects for these systems, see below). Fe atoms are positioned on top of selected oxygen or titanium atoms of the z'-TiO_x/Pt(111) structure (see Section III) as a starting configuration and then the system is left free to fully relax until the forces are smaller than 0.01 eV/Å per atom. It should be stressed that, as we deal with potentially polar systems, a dipole correction[32] is always applied to correct for the artificial electric field across the slab. It can also be added, however, that this correction in many cases did not change the qualitative features of Fe adsorption (see the discussion in Section V). STM images are simulated using the Tersoff−Hamann approach.[33]

The diffusion mechanisms and the corresponding energy barriers are calculated using a nudged elastic band (NEB) approach.[34] This method searches for the minimum energy path between two local minima by creating a fixed number of intermediate configurations (images) that are linked to each other by elastic springs. The image highest in energy does not feel the spring forces along the band; instead, the true force at this image along the tangent is inverted. In this way, the image tries to maximize its energy along the band, and thus when this image converges it is at the exact saddle point. The local minima singled out by the preliminary search are set as starting configurations of the NEB procedure, using a number of intermediate images ranging between 3 and 5.

Finally, Car−Parrinello (CP) simulations to test the stability of the structure with an Fe atom inside the defective hole of the z'-phase are also performed. The time step is set to 25 au (or 0.125 fs), the electron mass to 3500 au, a CP run consists of 500 minimization steps, 200 MD equilibration steps starting with null velocities at 300 K, and a variable number of production MD steps at the chosen temperature for a total simulation time of 5 ps using a Nosè thermostat for the kinetic energy of the electronic wave function.

III. The Adsorption Landscape

We start with a brief description of the adsorption template. The TiO_x/Pt(111) system presents a variety of phases; depending on the preparation conditions, several phases having different stoichiometry, structure and defects pattern can be isolated.[22] In particular, at low Ti coverage and in strongly reducing conditions an ultrathin wetting film is obtained, which, according to atomically resolved STM images, show a zigzag-like contrast, the z'-TiO_x/Pt(111) phase.[22,23] It has a commensurate rectangular unit cell of 14.4 × 16.6 Å^2 aligned along a <1$\bar{1}$0> direction of the Pt(111) surface and stoichiometry $Ti_{24}O_{30}$.[23] It is constituted of a $TiO_{1.25}$ monolayer with the Ti ions at the interface with the Pt(111) support and the O ions forming the topmost overlayer. Its structure can be described in terms of compact regions or infinite stripes running along a <1$\bar{1}$0> direction of the underlying metal support, linked to each other via defective troughs, see Figure 1. Within each stripe, the Ti atoms form a (111) pattern distorted in such a way that oxygen-tetracoordinated Ti atoms (indicated as $Ti_{4,ext}$ or $Ti_{4,int}$ in Figure 1 according to their position within the stripe) determine a zigzag-like motif (highlighted by a red line). The remaining Ti atoms are coordinated by only 3 oxygen atoms (indicated as Ti_3 in Figure 1) and are arranged in small (111) islands within the stripes. The troughs are constituted of irregular Ti_2O_3 units presenting two holes in each unit cell that expose the bare Pt(111) surface (indicated as *H* -sites in Figure 1). A variable degree of defectivity is observed depending on the postannealing time:[22,23] the structure of Figure 1 is obtained after 30 min annealing time at 673 K and has been tested as a template for the growth of metal clusters.[15,35] Further annealing however produces a gradual transition to a similar structure in which the holes are finally filled with Ti atoms, but the system is under kinetic control and a mixture of the two phases is usually observed.[23]

A. Single Atoms. The first point to be noted in describing the interaction of an Fe adatom with the z'-TiO_x surface is that (with the exception of the hole site) the most favorable adsorption configurations correspond to 3-fold face-centered cubic (fcc) hollow sites surrounded by O atoms not on-top of Ti ions, see Figure 1. These are also the only stable local minima, as the other possible adsorption configurations, corresponding to pseudoepitaxial hexagonal close-packed (hcp) stacking on-top of Ti ions, are higher in energy and represent saddle points in the energy hypersurface (see Section IV). Similarly, the positions on-top of or in bridge positions between O ions are found to be either maxima or nonstationary points at variance with the Au or Pd cases in which they correspond to local minima or saddle points.[15] The results of interaction energies and equilibrium heights (with respect to the Pt substrate) for the adsorption of Fe atoms on the z'-phase are collected in Table 1 where following three energy values are reported: the adhesion energy, E_{adh}, calculated by subtracting the energy of the isolated atom or dimer and that of the isolated substrate (the latter in the interacting configuration) from the total energy of the system and by taking the absolute value; the distortion energy, E_{dist}, calculated as the difference between the energy of the isolated substrate in the interacting configuration and its lowest-energy (optimized) configuration; the binding energy, E_{bnd}, obtained by subtracting the value of the distortion energy from the value of the adhesion energy and corresponding to the energy gain in absolute value achieved by carrying an atom from infinite distance to the interacting configuration. The relation $E_{bnd} = E_{adh} - E_{dist}$ holds.

From an analysis of Table 1, it can be drawn that the most attractive site is the defective hole with E_{bnd} = 4.66 eV, and that in general the binding energy increases in passing from the compact stripes (with $E_{bnd} \approx 2.25-2.39$ eV) to sites closer to the defective rims, with E_{bnd} =3.25 eV for R_2 or 3.45 eV for R_1 (see Figure 1 for the nomenclature of adsorption sites).

Also, it can be observed that an Fe atom adsorbed inside the hole is practically at the same height from the surface as the Ti ions, which are located at about 2.25 Å with respect to the Pt support, whereas Fe atoms in the other adsorption sites are farther from the surface. For comparison, an Fe atom is adsorbed in a hollow site of the bare Pt(111) surface with a binding energy of 3.5 eV and an equilibrium height of 1.57 Å; the presence of

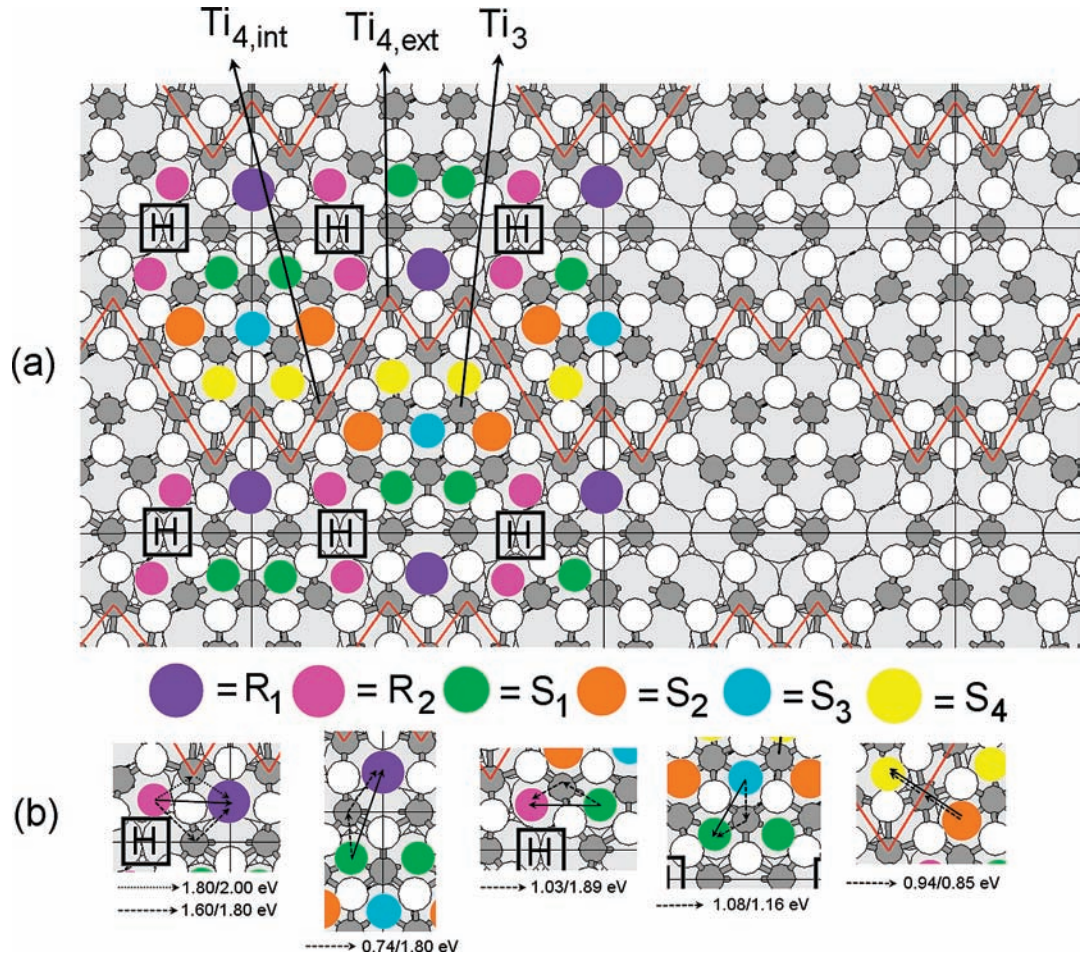

Figure 1. (a) Structure of the z'-TiO_x substrate and adsorption landscape. The bare substrate is shown on the right-hand-side, where the zigzag-like pattern of tetracoordinated Ti ions is highlighted with a red line. Ti atoms in dark gray, Pt atoms in light gray, O atoms in white. The adsorption sites for Fe atoms are shown in various colors in the picture, as detailed at the bottom. (b) Schematic representation of the various diffusion paths of Fe adatoms moving on the z'-TiO_x surface with the corresponding values of energy barriers (in eV) also reported in Table 3.

TABLE 1: Adsorption Sites for an Fe Adatom on the z'-TiO_x Phase (the Adopted Nomenclature Coincides with That Defined in Figure 1), Their Energetics (See the Text for a Definition of the Quantities, Adhesion Energy, E_{adh}, Distortion Energy, E_{dist}, and Binding Energy, E_{bnd}), the Equilibrium Height (h) of the Fe Atom with Respect to the Pt(111) Surface, and the Population Analysis for Majority- and Minority-Spin Orbitals, Respectively, Distinguished into s and d Components[a]

ads site	E_{adh}	E_{dist}	E_{bnd}	h	maj spin	min spin
H (Figure 2b)	5.29	0.63	4.66	2.12	4.84 d + 0.15 s	1.71 d + 0.12 s
R_1 (Figure 2c)	4.26	0.81	3.45	3.39	4.74 d + 0.18 s	1.83 d + 0.13 s
R_2	4.13	0.88	3.25	3.53		
S_1	2.99	0.60	2.39	3.72		
S_2	2.89	0.55	2.34	3.78		
S_3 (Figure 2d)	2.80	0.49	2.31	3.79	4.67 d + 0.13 s	2.19 d + 0.11 s
S_4	2.89	0.64	2.25	3.88		

[a] Energies in eV; heights in Å.

the oxidic template therefore increases both the Fe/Pt(111) interaction and the equilibrium height. A strong Fe/Pt(111) interaction in the hole site is confirmed by Car−Parrinello simulations conducted on the z'-TiO_x/Pt(111) phase containing an Fe atom in the hole site (see Section II for the computational details). Whereas in the case of a single Au atom adsorbed in the same site of the z'-phase Car−Parrinello simulations show a dynamic (entropic) rearrangement to a new structure that is the forerunner of a phase transformation from a rectangular to a hexagonal phase,[24] in the case of Fe no significant rearrangement is observed at both $T = 300$ and 600 K for a time lapse of at least 5 ps. This is certainly due to the smaller size of the Fe atom with respect to the Au atom that does not bounce against and produce strain on the hole's walls, but probably also to the different charge state (see Section V), that is partially positive in the Fe case and entails a stronger interaction with the Pt(111) surface.

The values of distortion energy E_{dist} are similar in the various adsorption configurations, and range between a minimum of 0.49 eV for the S_3 site to 0.88 eV for the R_2 site; larger values are found for the rim sites (R_1 and R_2) which possess a greater structural freedom and for which Fe adsorption implies a more appreciable reconstruction, whereas the scope of variation is more limited for the stripe sites (0.49−0.64 eV). Note again that the value for the hole site is within the latter range, confirming the smaller interaction of the Fe atom inside the defect with the oxide slab.

B. Dimers. A few configurations of Fe addimers have been considered, and their energetics is reported in Table 2, where in addition to the energetic quantities defined in Table 1 the difference between the binding energy of the dimer and the sum of the two binding energies for separated adatoms adsorbed in the two sites of the dimer is also given as Δ_{bnd}.

By analyzing the values of Δ_{bnd}, it can be observed that in several cases the adhesion energy of the dimer is very close to the sum of the adhesion energies of the separated adatoms. A

TABLE 2: Adsorption Sites of an Fe Addimer on the z'-TiO_x Phase (The Adopted Nomenclature Coincides with That Defined in Figure 1 with the Only Addition of S_3VS_3 That Corresponds to a Dimer Positioned Vertically on the S_3 Site) and Their Energetics (See the Text for a Definition of the Quantities, Adhesion Energy, E_{adh}, Distortion Energy, E_{dist}, and Binding Energy, E_{bnd})[a]

ads site	E_{adh}	E_{dist}	E_{met}	E_{bnd}	Δ_{bnd}
R_1-R_2 (Figure 2e)	8.20	2.36	0.69	6.53	−0.17
R_1-S_1 (Figure 2h)	7.67	2.00	0.29	5.96	+0.12
R_2-S_1 (Figure 2g)	6.57	1.93	0.91	5.55	−0.09
S_2-S_2 (distant)	5.80	1.11	0.01	4.70	+0.02
S_2-S_3 (Figure 2f)	4.85	1.43	1.16	4.58	−0.07
S_3VS_3	2.28	0.34	1.84	3.78	

[a] The metallic energy, E_{met}, is defined as the strength of the metallic Fe−Fe bond at the distance in the configuration interacting with the surface, while Δ_{bnd} is the difference between the binding energy of the addimer and the sum of the two binding energies for separated adatoms adsorbed in the two sites of the dimer, respectively. Energies in eV.

couple of points are worthwhile mentioning. (i) Some apparent attraction for dimers in which the two Fe atoms mirror each other across the trough, as for the R_1-S_1 pair in Figure 2h, due to a sinergic rearrangement of the oxide slab following adsorption; (ii) some apparent repulsion for dimers formed by adjacent atoms to be contrasted with a minor attraction for dimers in which the Fe atoms are both in stripe sites, but farther apart rather than adjacent, as for the S_2-S_2 (distant) pair. The repulsion found in case (ii) is expected on the basis of the charged character of Fe adatoms on this surface (see Section V) and should enhance the tendency of the Fe cluster growth on this system to be under kinetic control.

Finally, selected configurations with a vertical dimer, that is, a dimer in a configuration with its bond axis perpendicular to the surface, have been tested. They are found to be always higher in energy with respect to parallel configurations. As a representative example, a perpendicular Fe dimer in the S_3 site lies higher in energy by 0.92 eV with respect to a dimer formed by

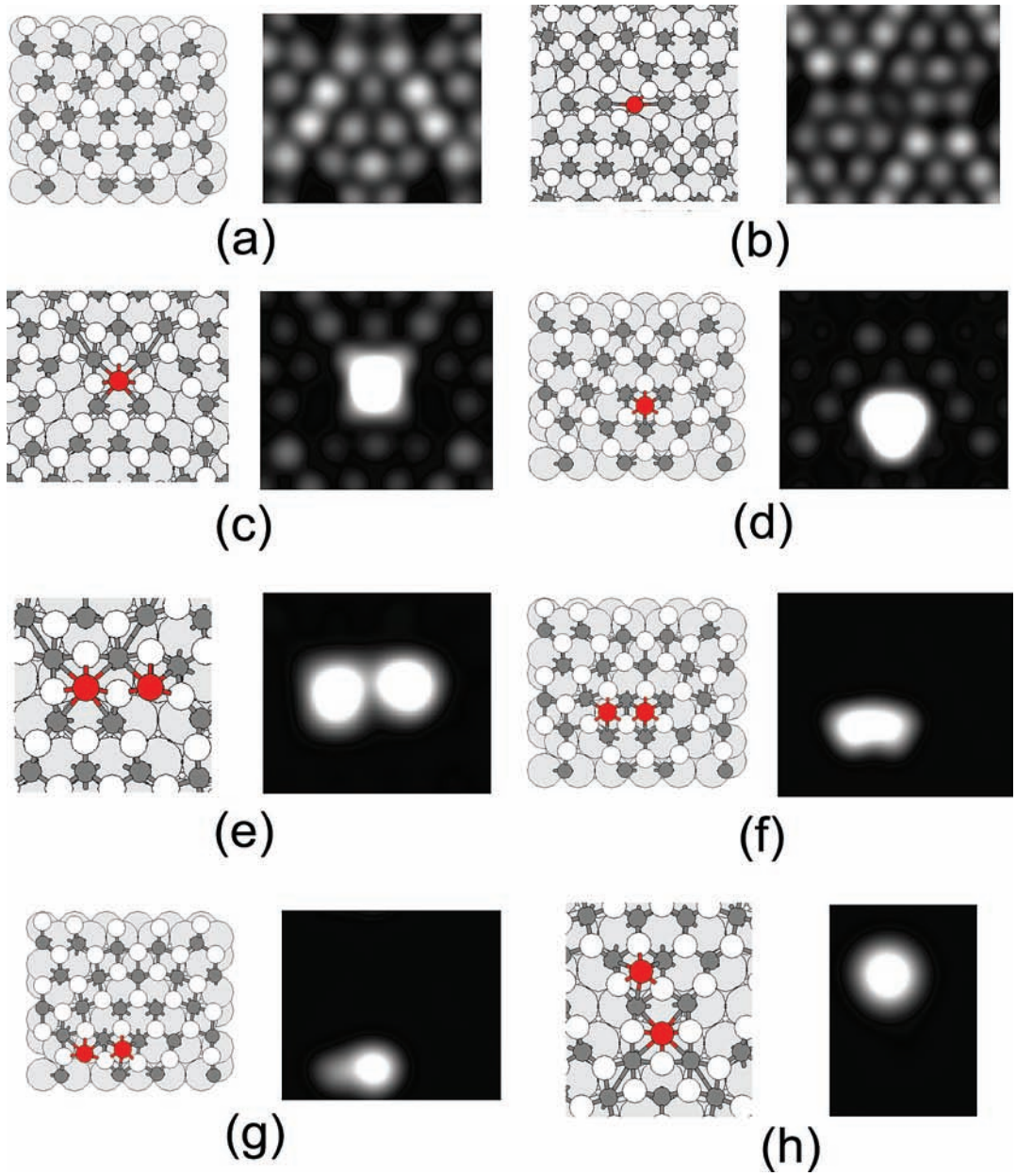

Figure 2. Structure and simulated STM images of the z'-TiO_x substrate (a) and of Fe adatoms (b−d) and addimers (e−h) adsorbed on it. The bias for the STM images is 1.55 eV for the bare substrate and the Fe adatoms, 0.89 eV for the Fe addimers.

TABLE 3: Forward and Backward Energy Barriers for Various Diffusion Paths of an Fe Atoms Moving on the z'-TiO_x Surface[a]

path	forward barrier	backward barrier	Δ_{dist}
$R_1 \rightarrow R_2$ (Ti 4)	1.80	2.00	0.78
$R_1 \rightarrow R_2$ (Ti 3)	1.60	1.80	0.91
$S_1 \rightarrow R_1$	0.74	1.80	0.91
$S_1 \rightarrow R_2$	1.03	1.89	0.98
$S_3 \rightarrow S_1$	1.08	1.16	0.81
$S_2 \rightarrow S_4$	0.94	0.85	0.70

[a] These diffusion mechanism are also graphically depicted in Figure 1b. Δ_{dist} is the distortion energy of the oxide slab at the saddle point. Energies in eV.

two Fe adatoms in (distant) S_2 positions (see Table 2). This is due to the strong adhesion of Fe to the surface, that exceeds the strength of the Fe−Fe bond. As a consequence, we predict a preferential two-dimensional (2D) rather than a three-dimensional (3D) growth of Fe clusters on this surface. For comparison, we report in Table 2 also the values of the metallic energy, E_{met}, that is, the strength of the Fe−Fe bond at the distance in the configuration interacting with the surface, to be contrasted with a value of 2.40 eV for E_{met} at the Fe_2 equilibrium distance of 1.97 Å, as predicted by the present computational approach.

IV. The Diffusion Energy Barriers

The results of the energy barriers for the diffusion of Fe atoms on the z'-phase are collected in Table 3, where the starting and final configurations and three values of energy are reported: the forward and backward barrier and the distortion energy of the oxide, Δ_{dist}, calculated as the difference between the energy of the isolated substrate in the saddle point configuration and its lowest-energy (optimized) configuration. The corresponding paths are also shown in Figure 1b.

From an analysis of Table 3 it can be drawn that the values of the diffusion barriers range around 0.7−1.1 eV when the Fe atom is moving over the stripe regions or from stripe sites into rim sites, but increase up to at least 1.6−2.0 eV for jumps starting from rim sites (R_1 and R_2) and reach a maximum of 2.5−3.2 eV when detrapping from the defective hole is involved (not shown in Figure 1b and Table 3). This is consistent with the larger values of adhesion energy observed for the rim sites and especially the hole site. It can be noted that the diffusion barrier values are much higher than those found for Au or Pd on the same system that range between 0.1 and 0.5 eV,[15,25] and point to a much greater importance of kinetic effects in the growth of Fe clusters on this surface.

It is interesting to underline that all saddle points can be described as adsorption on-top of Ti ions. Note also that the energy of the corresponding configurations is independent of the path used to reach them; when two different paths pass by the same saddle point, as in the case of the jumps $S_1 \rightarrow R_1$ and $R_1 \rightarrow R_2$ (passing atop a Ti_3), one can predict the energy barrier as the difference between the energies of the starting configurations and the energy of the saddle point. Rationalizing the actual values of energy barriers is however not straightforward. For example, the lowest-energy paths for diffusion are found to pass over Ti cations that would be expected to repel the slightly positively charged Fe atom (see Section V). This is even more true for the tetracoordinated Ti cations, that are more positively charged,[15] so that the saddle points corresponding to them should lye at higher energies with respect to those passing over tricoordinated Ti cations. This expectation is not met by the

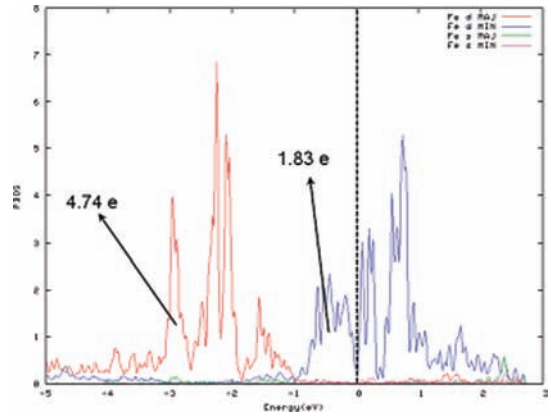

Figure 3. PDOS in arbitrary units for an Fe atom adsorbed on the site R_1 (only the Fe-projected contribution is shown). Energy abscissa in eV with the Fermi energy taken as zero.

results in Table 3, where the barrier for the jump $S_2 \rightarrow S_4$ is intermediate between that of the jump $S_3 \rightarrow S_1$ and that of the jump $S_1 \rightarrow R_1$. The reason is 2-fold. First, the Ti cations are not fully oxidized and still have electrons to bind the Fe atom; second, the Fe atom is close to four O ions instead of three in the saddle point configuration of the jump $S_2 \rightarrow S_4$. This analysis is confirmed by the fact that the values of distortion energy for the saddle points, Δ_{dist}, range between 0.70 and 0.98 eV and are thus on average larger than those for the local minima, E_{dist}, due to a larger rearrangement of both the Ti ion and the surrounding O ions in the transition configuration.

V. Fe Charge State and STM Images

To conclude the analysis of the results, it is of interest to ask oneself what is the charge state of the Fe atom interacting with the z'-TiO_x/Pt(111) surface. We recall from previous work that Pd is neutral and that Au is neutral or negatively charged.[15] In contrast, from a post-scf analysis of the electron density we find that Fe is positively charged. The values of the total charge, reported for selected cases in Table 1 as decomposed into s- and d-contributions, range from 1.1−1.2 e for Fe atoms in the troughs or rims to ∼0.9 e for Fe atoms in the stripes, respectively. It can be noted from Table 1 that this charging is realized essentially as a depletion of electron density in the s-orbitals, while the d-space orbitals consistently host 6.5−6.9 electrons. This is confirmed by a plot of the projected density of states (PDOS) for an Fe atom adsorbed on a R_1 site, shown in Figure 3. It can be observed that the majority-spin d-band is fully occupied and lies ∼2 eV below the Fermi energy, whereas the minority-spin d-band is partially occupied with ∼2 electrons, so that the total spin of the system is $S = 3/2$. The positive charge state of Fe has however a slight effect on the adsorption phenomenology, as confirmed by the minor repulsion between adjacent Fe dimers from the results of Table 2, and the fact that the values of the charges found in the case of neighboring dimers are only slightly modified with respect to the situation of isolated adatoms, as we have verified in the case of a dimer formed by two Fe atoms adsorbed in the S_2 and S_3 sites, that is, the horizontal configuration corresponding to the strongest metallic bond.

Moreover, we have evaluated the change in the dipole moment of the system before and after adsorption of a single Fe atom (on a S_3 site, but similar results are found in other cases) by plotting the energy of the system as a function of an applied electric field and by taking the numerical derivative of the energy with respect to the field value at zero field. Note

that a dipole correction[32] is always applied to cancel spurious contributions due to electrostatic interactions between replicated cells. We found that the bare z'-TiO_x template has a dipole moment across the slab of 1.84 au It must be stressed that although the atomic stacking of the oxide film is $Pt-Ti^+-O^-$, the direction of this dipole moment is such that its negative pole is on the metal slab and the positive one on the oxide slab. The value of the dipole moment then increases to 2.45 au after Fe adsorption. This counterintuitive result (one could in fact expect that the direction of the dipole moment of the oxide film is Ti^+-O^-, that it determines the total dipole moment of the system, and that the presence of a positively charged Fe atom on top of the O overlayer opposes this dipole moment) is due in part to the fact that the difference in height between the Fe atom and the O overlayer is not large (as mentioned above, the Ti layer is at about 2.15 Å above the Pt(111) surface, while the O overlayer is positioned at about 2.90 Å above the Pt support; see also Table 1), and especially to the fact that the free, unsupported oxide layer has a negligible dipole moment to begin with, so that when it is deposited on the Pt(111) surface the prevailing effect is a charge transfer from the oxide to the metal slab due to the higher electronegativity of the latter. When an Fe atom is then adsorbed, despite the fact that the oxygen atoms closest to Fe increase their negative charge, the overall change is directed by the additional effect of the positive Fe species. We note in passing that neglecting the dipole correction does not qualitatively change the qualitative picture; the total energies of the z'-TiO_x slab with and without the dipole correction differ by 0.05 and 0.08 eV before and after adsorption of an Fe atom on a stripe site, respectively. The adhesion energy of an Fe adatom on a stripe site is thus modified by only 0.03 eV by the dipole correction.

Finally, in Figure 2 we show simulated STM images of single Fe adatoms and addimers adsorbed on the z'-TiO_x phase in selected sites. These correspond to plotting the PDOS at a given bias with respect to the Fermi energy in a plane lying at 2 Å above the oxygen layer, in the case of the bare titania phase, or above the topmost Fe atom, in the case of a system with an adsorbed Fe adatom or addimer. In Figure 2a, it can be observed the typical zigzag-like pattern of the bare z'-TiO_x substrate;[23] in Figure 2b the fact that the Fe atom in the defective hole is encompassed within the oxide slab and apparently does not contribute much to the STM signal, whereas in Figures 2c,d the bright spots corresponding to Fe atoms adsorbed in R_1 and S_3 sites, respectively, are evident. In Figure 2e−h, the STM images relative to the adsorption of Fe dimers are shown. A variety of possibility is found. For the adsorption in two rim sites (R_1 and R_2; see Figure 2e), two well distinct spots of similar brightness are observed. The two spots are still comparable in size, but are more diffuse and somewhat merged in the case of adsorption in two stripe sites (S_2 and S_3; see Figure 2f). A dissimmetric situation is instead found in the case that one Fe atom is adsorbed in a stripe site and another in a rim site: the spot associated with the former appears much brighter and bigger (R_2 and S_1; see Figure 2g) or nearly unique (S_1 and R_1; see Figure 2h). This effect is partially an artifact due to plotting the PDOS in a plane 2 Å above the topmost Fe atom (i.e., that adsorbed in a stripe site) in a constant-height rather than a constant-current mode as in the experiment, but it nevertheless witnesses an asymmetry in the strength of the corresponding STM features.

VI. Conclusions

Accurate theoretical information on basic dynamic processes[36] is essential to understand and predict growth processes. In the present article, the adsorption landscape and the diffusion energy barriers for Fe adatoms adsorbed on an ultrathin titania film, the z'-$TiO_{1.25}$/Pt(111) phase, and the energetics of Fe addimers on the this film are studied via density functional simulations. From the analysis of the computational results, several observations and conclusions can be drawn.

First, we find a strong adhesion of Fe to the oxide phase as a main ruling factor. This makes that 3-fold hollow fcc sites are the preferred adsorption sites for Fe atoms, that the adsorption energetics ranges between 2.3 and 4.7 eV for adatoms and proportionally for addimers, that the energy barriers for diffusion are substantial (∼0.7−2.0 eV) and pass through saddle points on top of Ti ions, and that Fe addimers prefer horizontal to vertical configurations.

Second, within this panorama we find a modulation of the adsorption and diffusion energetics with a general increase of adhesion and detrapping energy values in going from the compact regions (stripes) to the more defective regions (rims or troughs) of the oxide phase. This increase reaches its maximum at the hole site, where an adsorbed Fe atom is now encompassed within the titania film and its interaction with the Pt(111) surface is enhanced with respect to the metal-on-metal case, despite a larger equilibrium distance. It can however be noted that in order to reach this energetically most favorable situation an Fe atom has to overcome substantial energy barriers, a fact that might also explain previous difficulties encountered in rationalizing the growth of Fe clusters on other ultrathin oxides.[16,17]

These results are rationalized via a post-scf analysis of the electron density, showing that the Fe atoms are positively charged by the interaction with the surface. This explains the bright spots associated with them in STM images at positive bias, the increase in the slab dipole moment after Fe adsorption, and the slight repulsion among Fe adatoms adsorbed in adjacent sites on the stripe regions. Note that, surprisingly, the dipole moment of the z'-$TiO_{1.25}$ /Pt(111) phase before Fe adsorption is such that its negative pole is on the metal slab, and the positive one on the oxide slab.

All these observations concurrently lead to the conclusion that the growth of Fe clusters on this phase will be strongly affected by the kinetics of the growth process with a preference for 2D rather than 3D configurations and the tendency toward irregular morphologies. Moreover, reaching the thermodynamic régime might not be simply achieved by increasing the temperature, as this could activate higher-energy phenomena such as an intermixing of Fe with the ultrathin oxide monolayer.[37,38] A detailed comparison with experimental results on this system, that validates all the previous theoretical considerations, will be published elsewhere.

It can finally be added that analogous calculations performed on the adsorption and diffusion of a Co atom (unpublished results) support entirely analogous conclusions, so that the behavior of Fe can be taken as representative of a whole class of transition metals.

Acknowledgment. We thank Luca Gavioli and Gaetano Granozzi for many enlightening discussions on the experimental results on these systems and a long-standing collaboration. Financial support from the SEPON project within the ERC Advanced Grants (European Community Seventh Framework

Project, contract no. ERC-2008-AdG-227457) is gratefully acknowledged.

References and Notes

(1) Baletto, F.; Ferrando, R. *Rev. Mod. Phys.* **2005**, *77*, 371.
(2) Courty, A.; Henry, A. I.; Goubet, N.; Pileni, M.-P. *Nat. Mater.* **2007**, *6*, 900.
(3) Chen, J.; Lim, B.; Lee, E. P.; Xia, Y. *Nano Today* **2009**, *4*, 81.
(4) Henry, C. R. *Prog. Surf. Sci.* **2005**, *80*, 92.
(5) Freund, H. J. *Surf. Sci.* **2002**, *500*, 271.
(6) Goniakowski, J.; Mottet, C.; Noguera, C. *Phys. Status Solidi B* **2006**, *243*, 2516.
(7) Schebarchov, D.; Hendy, S. C.; Polak, W. *J. Phys.: Condens. Matter* **2009**, *21*, 144204.
(8) Xu, L.; Henkelman, G.; Campbell, C. T.; Jönsson, H. *Phys. Rev. Lett.* **2005**, *95*, 146103.
(9) Barcaro, G.; Fortunelli, A.; Nita, F.; Ferrando, R. *Phys. Rev. Lett.* **2005**, *95*, 246103.
(10) Ferrando, R.; Fortunelli, A. *J. Phys.: Condens. Matter* **2009**, *21*, 264001.
(11) Sterrer, M.; Fischbach, E.; Risse, T.; Freund, H. J. *Phys. Rev. Lett.* **2005**, *94*, 186101.
(12) Surnev, S.; Ramsey, M. G.; Netzer, F. P. *Prog. Surf. Sci.* **2003**, *73*, 117.
(13) Goniakowski, J.; Finocchi, F.; Noguera, C. *Rep. Prog. Phys.* **2008**, *71*, 016501.
(14) Chen, M. S.; Goodman, D. W. *J. Phys.: Condens. Matter* **2008**, *20*, 264013.
(15) Barcaro, G.; Fortunelli, A.; Granozzi, G. *Phys. Chem. Chem. Phys.* **2008**, *10*, 1876.
(16) Schmid, M.; Kresse, G.; Buchsbaum, A.; Napetschnig, E.; Gritschneder, S.; Reichling, M.; Varga, P. *Phys. Rev. Lett.* **2007**, *99*, 196104.
(17) Hamm, G.; Becker, C.; Henry, C. R. *Nanotechnology* **2006**, *17*, 1943.
(18) Repp, J.; Meyer, G.; Olsson, F. E.; Persson, M. *Science* **2004**, *305*, 493.
(19) Pacchioni, G.; Giordano, L.; Baistrocchi, M. *Phys. Rev. Lett.* **2005**, *94*, 226104.
(20) Sterrer, M.; Risse, T.; Heyde, M.; Rust, H. P.; Freund, H.-J. *Phys. Rev. Lett.* **2007**, *98*, 206103.
(21) Nilius, N.; Ganduglia-Pirovano, M. V.; Kulawik, V. B. M.; Sauer, J.; Freund, H.-J. *Phys. Rev. Lett.* **2008**, *100*, 096802.
(22) Sedona, F.; Rizzi, G. A.; Agnoli, S.; Xamena, F. X. L. I.; Papageorgiou, A.; Ostermann, D.; Sambi, M.; Finetti, P.; Schierbaum, K.; Granozzi, G. *J. Phys. Chem. B* **2005**, *109*, 24411.
(23) Sedona, F.; Granozzi, G.; Barcaro, G.; Fortunelli, A. *Phys. Rev. B* **2008**, *77*, 115417.
(24) Barcaro, G.; Fortunelli, A.; Sedona, F.; Granozzi, G. *J. Phys. Chem. C* **2009**, *113*, 1143.
(25) Rizzi, G. A.; Sedona, F.; Artiglia, L.; Agnoli, S.; Barcaro, G.; Fortunelli, A.; Cavaliere, E.; Gavioli, L.; Granozzi, G. *Phys. Chem. Chem. Phys.* **2009**, *11*, 2177.
(26) http://www.quantum-espresso.org (last accessed September 28, 2009).
(27) Vanderbilt, D. *Phys. Rev. B* **1990**, *41*, 7892–7895.
(28) Perdew, J. P.; Burke, K.; Ernzerhof, M. *Phys. Rev. Lett.* **1996**, *77*, 3865.
(29) Aprà, E.; Fortunelli, A. *J. Mol. Struct. (Theochem)* **2000**, *501*, 251.
(30) Wang, Y.; Doren, D. J. *Solid State Commun.* **2005**, *136*, 186.
(31) Finazzi, E.; Valentin, C. D.; Pacchioni, G.; Selloni, A. *J. Chem. Phys.* **2008**, *129*, 15411.
(32) Bengtsson, L. *Phys. Rev. B* **1999**, *59*, 12301.
(33) Tersoff, J.; Hamann, D. R. *Phys. Rev. Lett.* **1983**, *50*, 1998.
(34) Henkelman, G.; Uberuaga, B. P.; Jonsson, H. *J. Chem. Phys.* **2000**, *113*, 9901.
(35) Sedona, F.; Agnoli, S.; Fanetti, M.; Kholmanov, I.; Cavaliere, E.; Gavioli, L.; Granozzi, G. *J. Phys. Chem. C* **2007**, *111*, 8024–8029.
(36) Maciel, G. S.; Cappelletti, D.; Grossi, G.; Pirani, F.; Aquilanti, V. *Adv. Quantum Chem.* **2008**, *55*, 311.
(37) Qin, Z.-H.; Lewandowski, M.; Sun, Y.-N.; Shaikhutdinov, S.; Freund, H.-J. *J. Phys. Chem. C* **2008**, *112*, 10209.
(38) Parteder, G.; Allegretti, F.; Surnev, S.; Netzer, F. *Surf. Sci.* **2008**, *602*, 2666.

JP904998C